Supplemental Document

Biomedical Optics EXPRESS

Deep learning-based adaptive optics for light sheet fluorescence microscopy: supplement

MANI RATNAM RAI,[1,2] CHEN LI,[1,2] H. TROY GHASHGHAEI,[2,3] AND ALON GREENBAUM[1,2,4,*]

[1] *Joint Department of Biomedical Engineering, North Carolina State University and University of North Carolina at Chapel Hill, Raleigh, NC 27695, USA*
[2] *Comparative Medicine Institute, North Carolina State University, Raleigh, NC 27695, USA*
[3] *Department of Molecular Biomedical Sciences, North Carolina State University, Raleigh, NC 27695, USA*
[4] *Bioinformatics Research Center, North Carolina State University, Raleigh, NC 27695, USA*
[*] *greenbaum@ncsu.edu*

Supplement DOI: https://doi.org/10.6084/m9.figshare.22954616

Parent Article DOI: https://doi.org/10.1364/BOE.488995

Supplementary information

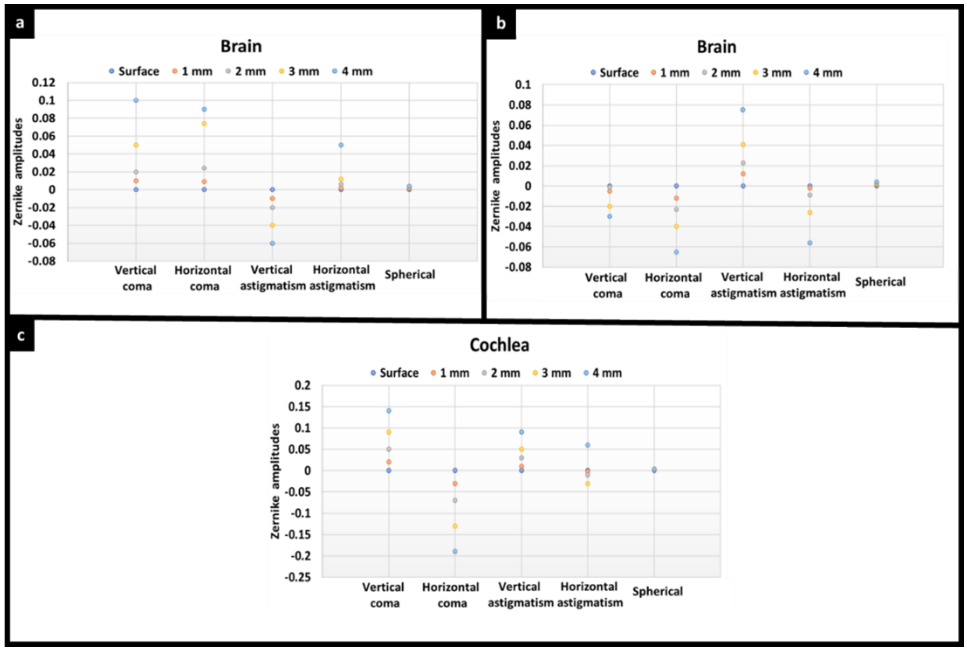

Fig. S1 Depth-dependent Zernike amplitudes for (a-b) two rat brains and (c) pig cochlea. Please note that the values provided are highly dependent on the quality of the clearing and age of the sample. Therefore, these values may vary from sample to sample, as well as within a sample depending on the spatial location that is imaged.

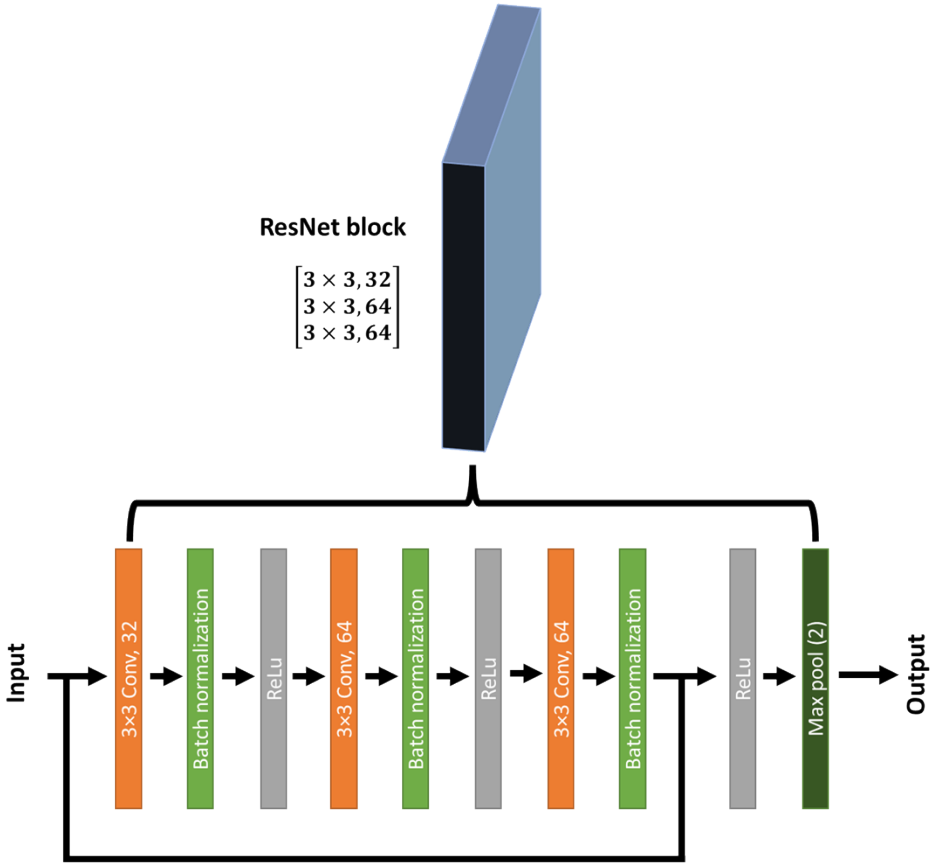

Fig. S2 The architecture of a single ResNet block.

Zernike Amplitudes						Mean	STD
Z_4 (Vertical Coma)	-0.0590	-0.0572	-0.0545	-0.0504	0.0505	-0.0543	0.0040
Z_5 (Horizontal Coma)	0.0216	0.0297	0.0296	0.0249	0.0280	0.0267	0.0035
Z_6 (Vertical Astigmatism)	0.0414	0.0442	0.0492	0.0479	0.0491	0.0464	0.0034
Z_7 (Horizontal Astigmatism)	-0.0058	-0.0071	-0.0108	-0.0045	-0.0137	-0.0084	0.0038
Z_{10} (Spherical)	0.0114	0.0113	0.0114	0.0107	0.0105	0.0111	0.0004

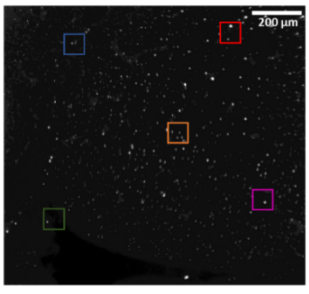

Fig. S3 The estimated Zernike amplitudes for different locations within the FOV (color coded), the mean and standard deviation (STD) are shown.

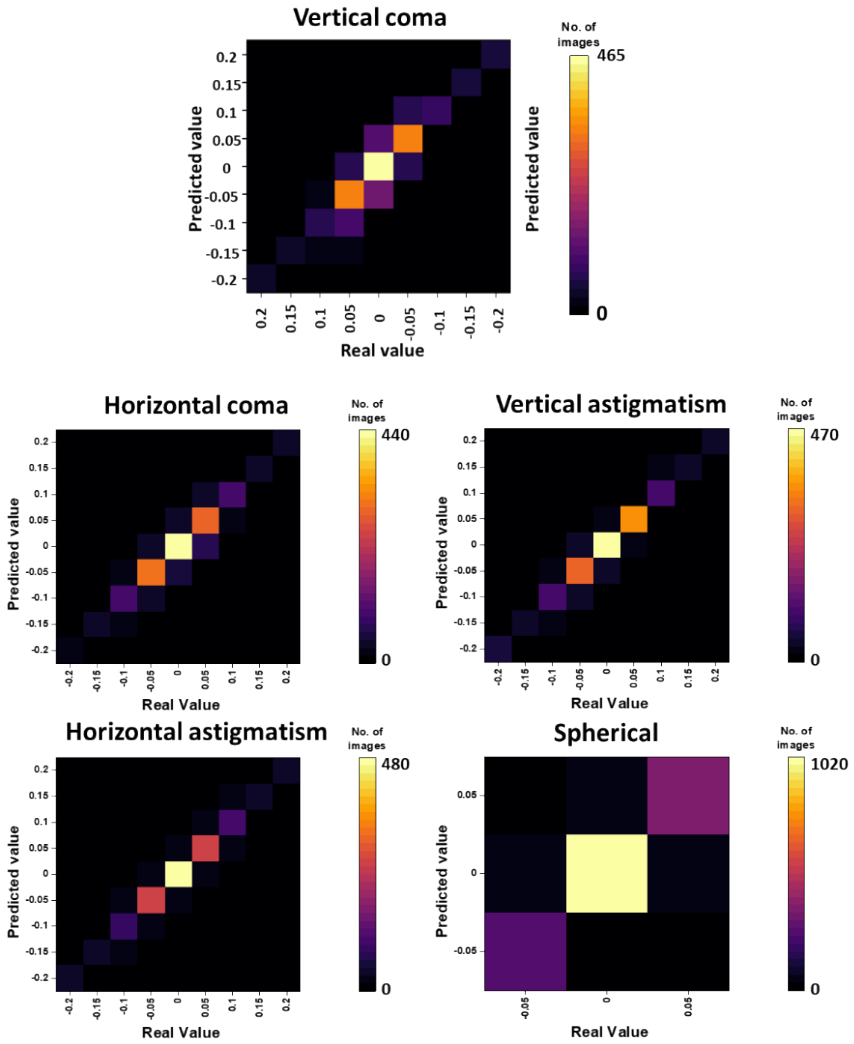

Fig. S4 Confusion matrices for different aberration types. The matrices were obtained from the *non-shared* network.

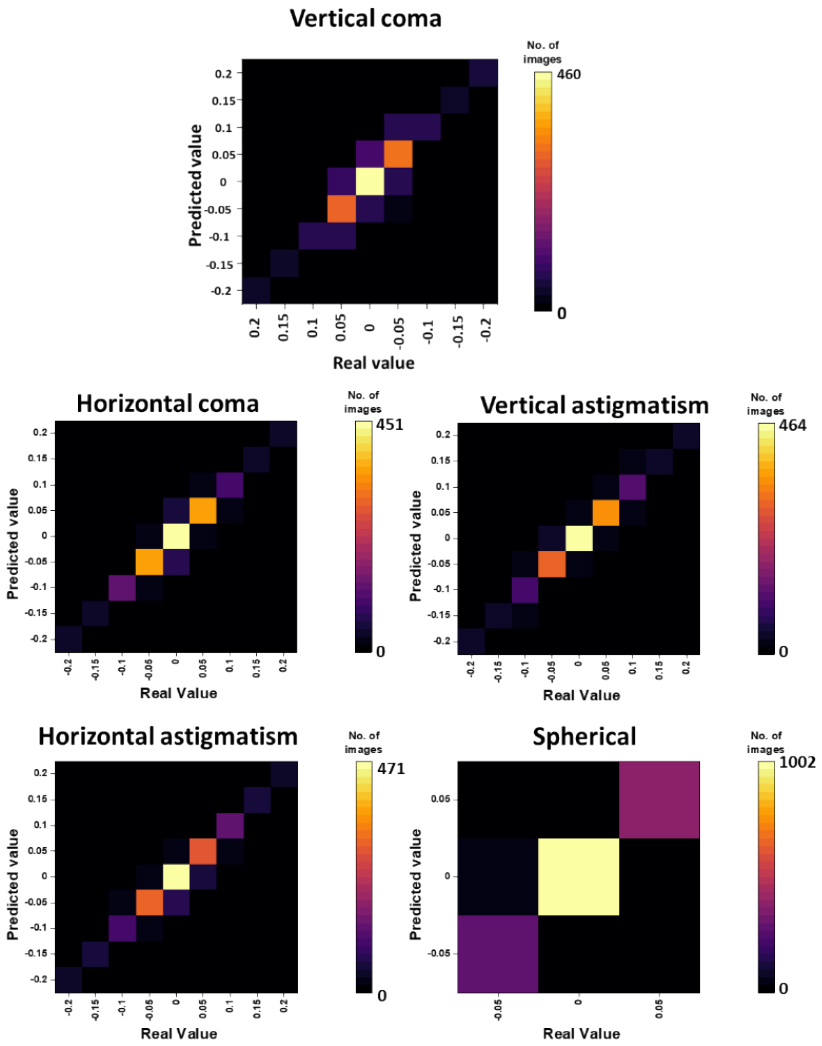

Fig. S5 Confusion matrices for different aberration types. The matrices were obtained from the *shared* network.

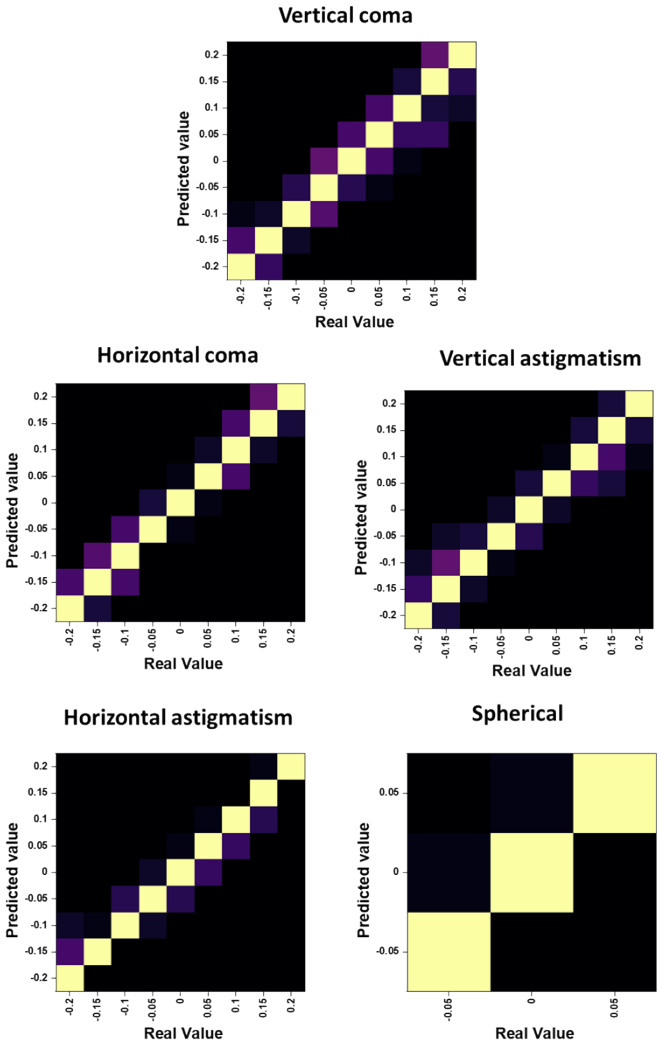

Fig. S6 Normalized confusion matrices for different aberration types. The matrices were obtained from the non-*shared* network.

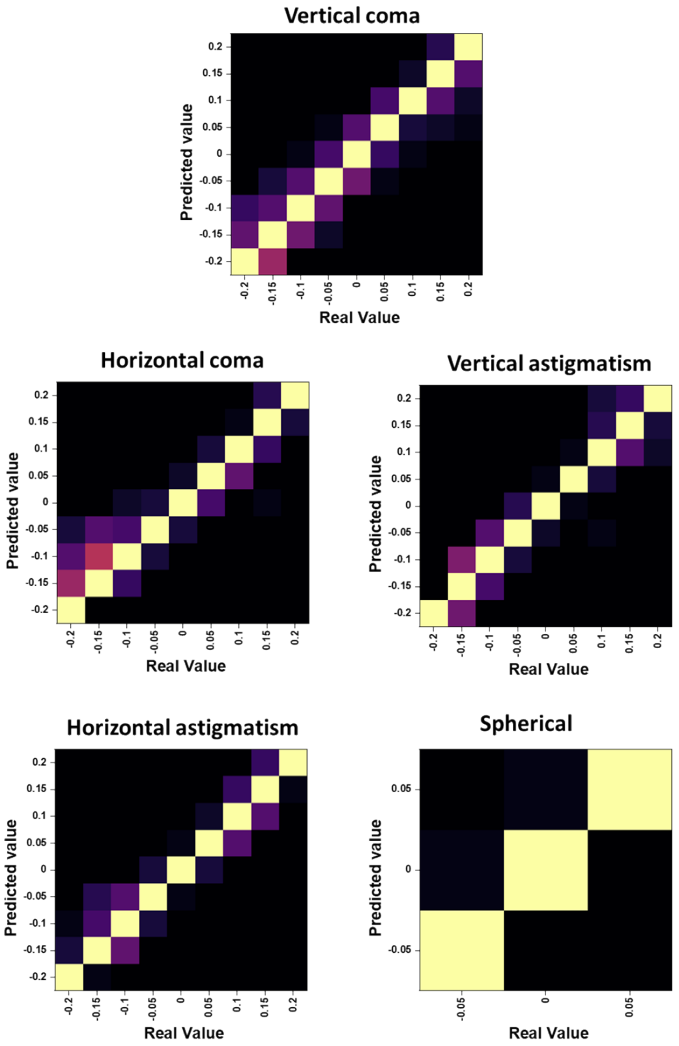

Fig. S7 Normalized confusion matrices for different aberration types. The matrices were obtained from the *shared* network.

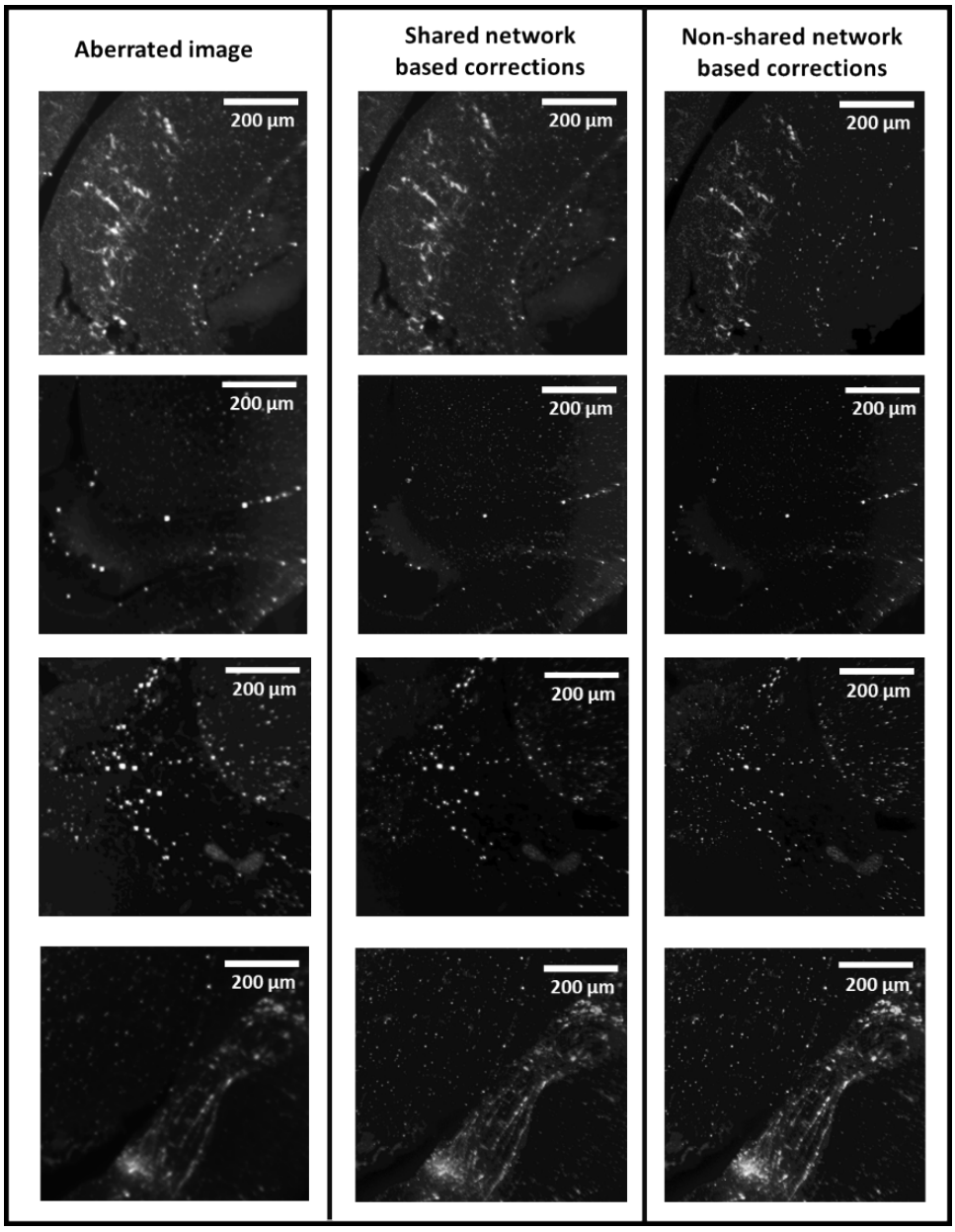

Fig. S8 Additional examples of aberration correction using the *non-shared* and *shared* networks. The figure shows data acquired from tissue cleared rat brains.